Substituent effects on the structure–property relationship of unsymmetrical methyloxy and methoxycarbonyl phthalocyanines: DFT and TDDFT theoretical studies

Lijuan Zhang, Dongdong Qi, Luyang Zhao, Yongzhong Bian*, Wenjun Li*

Department of Chemistry, University of Science and Technology Beijing, Beijing 100083, China

ABSTRACT

Density functional theory (DFT) and time-dependent density functional theory (TD-DFT) calculations were carried out to simulate the molecular and electronic structures together with the electronic absorption spectra of a series of peripheral methyloxy/methoxycarbonyl substituented phthalocyanines $M[Pc(\beta\text{-OMe})_{2n}(\beta\text{-COOMe})_{8-2n}]$ (M = 2H, Zn; n = 0, 1, 2, 3, and 4). Fragment charge distribution and electrostatic potential analysis indicate that the presence of electron-withdrawing and -donation groups leads to the redistribution of charges and obvious polarization effects to the unsymmetrical phthalocyanine series. Peripheral methyloxy/methoxycarbonyl groups introduced onto phthalocyanine ring were revealed to destroy the degeneracy of LUMOs, resulting in significant Q-band splitting for the unsymmetrical phthalocyanine compounds. In addition, metal-free and zinc phthalocyanine compounds display similar electronic structures and absorptions due to the almost none contribution of the zinc atom or inner hydrogens to the frontier molecular orbitals. The microscopic mechanism of the UV–Vis spectra has been clarified on the basis of multi-band photon-induced electron transference. These theoretical studies would be helpful for the molecular design of novel unsymmetrical phthalocyanines.
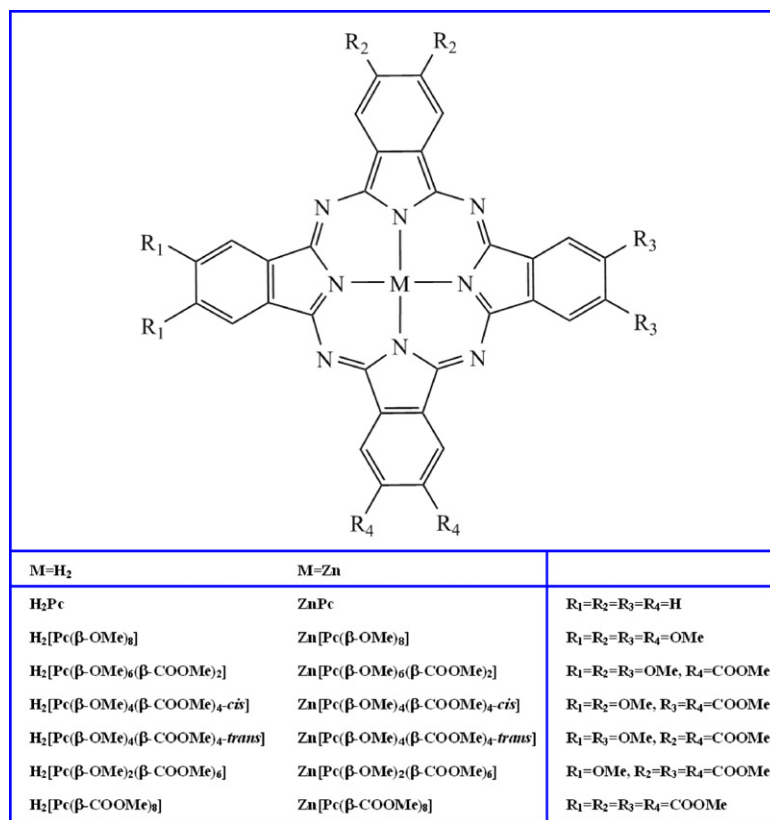
1. Introduction

Phthalocyanines (Pcs), derivatives of the aromatic tetraazaporphyrins, have been an important class of molecular functional materials due to their intriguing physic-chemical properties [1]. Tremendous efforts have been paid towards the development of new phthalocyanine molecular materials and their applications. In the past century, some symmetrical phthalocyanines that are able to be synthesized in relatively easy manner have been intensively theoretically and experimentally investigated [2,3]. In particular, those simultaneously possessed peripheral electron-donating and withdrawing groups have been continuously attracting research interests due to their potential applications in the fields of nonlinear optical materials [4], photodynamic therapy [5] and dye-sensitized solar cells [6] associated with their unique push–pull electronic structure. In dye-sensitiezed solar cells (DSSCs), unsymmetrical phthalocyanines with π-delocalized electron-acceptors are considered as a hopeful class of electron directional transferring skeletons from the organic dyes to TiO₂ clusters with high efficiency [7–9], which actually also have great potential applications in second-order nonlinear optical (NLO) materials [4,10].

Along with the significant progress in molecular material chemistry, new methods have been developed for synthesizing various kinds of unsymmetrical phthalocyanines in recent years [11–13]. Kobayashi and co-workers have synthesized a series of low-symmetry tetrapyrrole analogues with proton-induced unsymmetrical electron floating and multi-band photon absorption properties associated with their unique push–pull electronic structure [14–16]. Recently, another series of unsymmetrical phthalocyanines with the central phthalocyanine chromophore kept unchanged but possessing different electron-donating/withdrawing substituents at the periphery have been reported by Jiang and co-workers [11,17–19]. Despite even the quantum chemistry calculations were employed towards the objective-oriented design and synthesis of novel unsymmetrical phthalocyanine compounds [7,8], there still exists no systematical theoretical study on the electronic structure, electronic distribution, molecular orbitals, photon-induced electron transference, and electronic absorption spectra of a full series of unsymmetrical phthalocyanines.

In the present paper, density functional theory (DFT) calculations with B3LYP and time dependent density functional theory (TDDFT) calculations with BPW91 are applied to simulate the molecular structures, atomic charge distributions, molecular orbitals, and electronic absorption spectra of a full series of unsymmetrical metal-free and zinc phthalocyanines

* Corresponding authors. Tel.: +86 10 6233 4509; fax: +86 10 6233 2462.
E-mail addresses: yzbian@ustb.edu.cn (Y. Bian), wjli@sas.ustb.edu.cn (W. Li).

M=H₂	M=Zn	
H₂Pc	ZnPc	R₁=R₂=R₃=R₄=H
H₂[Pc(β-OMe)₈]	Zn[Pc(β-OMe)₈]	R₁=R₂=R₃=R₄=OMe
H₂[Pc(β-OMe)₆(β-COOMe)₂]	Zn[Pc(β-OMe)₆(β-COOMe)₂]	R₁=R₂=R₃=OMe, R₄=COOMe
H₂[Pc(β-OMe)₄(β-COOMe)₄-*cis*]	Zn[Pc(β-OMe)₄(β-COOMe)₄-*cis*]	R₁=R₂=OMe, R₃=R₄=COOMe
H₂[Pc(β-OMe)₄(β-COOMe)₄-*trans*]	Zn[Pc(β-OMe)₄(β-COOMe)₄-*trans*]	R₁=R₃=OMe, R₂=R₄=COOMe
H₂[Pc(β-OMe)₂(β-COOMe)₆]	Zn[Pc(β-OMe)₂(β-COOMe)₆]	R₁=OMe, R₂=R₃=R₄=COOMe
H₂[Pc(β-COOMe)₈]	Zn[Pc(β-COOMe)₈]	R₁=R₂=R₃=R₄=COOMe

Scheme 1. Schematic molecular structures of $M[Pc(\beta\text{-OMe})_{2n}(\beta\text{-COOMe})_{8-2n}]$ (M = 2H, Zn; n = 0, 1, 2, 3, and 4).

simultaneously possessing electron-donating methyloxy and electron-withdrawing methoxycarbonyl substitutents at the phthalocyanine periphery, namely $M[Pc(\beta\text{-OMe})_6(\beta\text{-COOMe})_2]$, $M[Pc(\beta\text{-OMe})_4(\beta\text{-COOMe})_4\text{-}cis]$, $M[Pc(\beta\text{-OMe})_4(\beta\text{-COOMe})_4\text{-}trans]$, and $M[Pc(\beta\text{-OMe})_2(\beta\text{-COOMe})_6]$, Scheme 1. For the purpose of comparative study, symmetrical analogues MPc, $M[Pc(\beta\text{-OMe})_8]$ and $M[Pc(\beta\text{-COOMe})_8]$ (M = 2H, Zn) have also been involved in the present study. As expected, comparative and systematic studies easily reveal the influence of the number and position of substituents on the structures and properties of the metal-free and zinc phthalocyanines. The present result dealing with the detailed structures, charge distribution, spectroscopic properties, photon-induced electron transference, and substitution effect of a full series of peripherally methyloxy/methoxycarbonyl substituented compounds $M[Pc(\beta\text{-OMe})_{2n}(\beta\text{-COOMe})_{8-2n}]$ (M = 2H, Zn; n = 0, 1, 2, 3, and 4) will be useful for understanding the relationship between the molecular structure and properties of unsymmetrical phthalocyanine derivatives.

2. Computational details

The hybrid generalized gradient approximation (hGGA) functional B3LYP has been proved suitable for the geometry optimization of porphyrins, phthalocyanines, as well as their various metal analogues [20–22]. As a consequence, in the present study B3LYP was employed for conducting the geometry optimization of all the series of metal free and zinc compounds of phthalocyanines. However, B3LYP was revealed to overestimate the transition energies for this type of large conjugated systems, while generalized gradient approximation (GGA) method significantly improves the agreement between theoretical and experimental results [23–25]. As a result, GGA functional BPW91 was employed to carry out the transition energy calculation of

corresponding phthalocyanine compounds. In order to verify the reliability of our TDDFT computation result, calculations at five different levels of theory for $Zn[Pc(\beta\text{-OMe})_8]$ were performed and the results given in The Validity of the Functional BPW91 Section of Supporting Information validate the BPW91 method employed in the present case.

All geometries were optimized at the DFT method of B3LYP functional with Becke's three-parameter hybrid exchange [26] and Lee–Yang–Parr non-local correlation [27]. The Berny algorithm using redundant internal coordinates [28] was employed in energy minimization and the default cutoffs were used throughout. No imaginary vibration was predicated in the following frequency calculations of the IR vibration spectroscopy, indicating that the energy-minimized structures for all of the complexes are true energy minima. In an attempt to further understand the push-pull effect, natural bond orbital (NBO) analysis [29] was carried out with NBO 3.1 [30] in Gaussian 03 program [31] on the basis of the minimized structures.

The electronic structures and electronic absorption spectra were calculated using DFT method of Beck's exchange functional [32] and Perdew–Wang correlation functional (BPW91) [33]. The configurations of transition models were calculated using the SWizard program, revision 4.6 [34,35]. In all cases, the LanL2DZ basis set for Zn atoms, 6-31+G(d) basis set for oxygen atoms, and 6-31G(d) basis set for all the other atoms were employed. All calculations were carried out using the Gaussian 03 program [31] on an IBM P690 system housed at Shandong Province High Performance Computing Center.

The total electron density difference between ground and excited states ($\sum f_{m \to n}$) is calculated by the molecular orbital electron density difference $f_{m \to n} = c_{m \to n}^2 (\rho_n - \rho_m) / \sum c_{m \to n}^2$, where ρ_n and ρ_m are the electron density of the two molecular orbitals relative to the electron transition model of $MO(m) \to MO(n)$, $c_{m \to n}$ is the orthogonal coefficient in the TD-DFT equation, and then
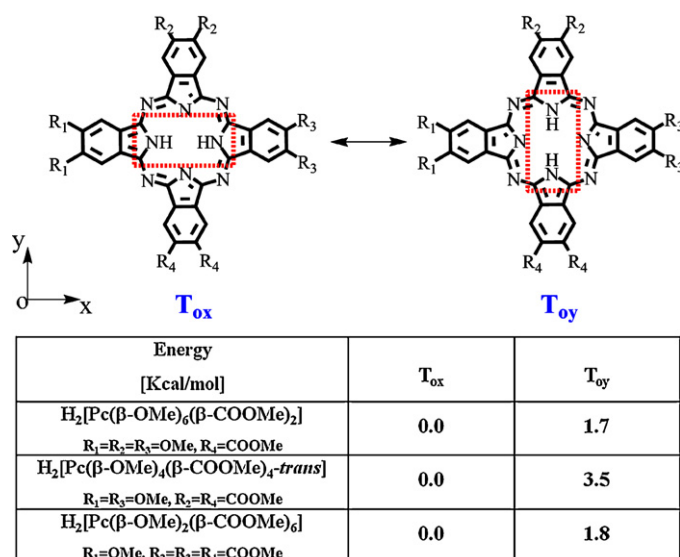
Fig. 1. Toutomeric forms of $H_2[Pc(\beta\text{-OMe})_6(\beta\text{-COOMe})_2]$, $H_2[Pc(\beta\text{-COOMe})_4\text{-}trans]$, and $H_2[Pc(\beta\text{-OMe})_2(\beta\text{-COOMe})_6]$, as well as their relative energies.

$c_{m\to n}^2/\sum c_{m\to n}^2$ can be considered as the contribution of this electron transition model to this absorption peak [25]. The electron density difference between ground and excited states is the linear combination of various electron transition models. Also for the reason of time efficiency, only the electron transition models with the configuration larger than 5.0% are taken into account. The electron density difference of 5.0×10^{-4} e×a.u.^{3}.

The electrostatic potentials (EPs) of $Zn[Pc(\beta\text{-OMe})_{2n}(\beta\text{-COOMe})_{8-2n}]$ ($n = 0, 1, 2, 3,$ and 4) are calculated by

$$V(\vec{r}) = V(\vec{r})_{\text{nucleus}} + V(\vec{r})_{\text{electron}} = \sum_A \frac{q_A}{|\vec{r} - \vec{R}_A|} - \int \frac{\rho(\vec{r}')}{|\vec{r} - \vec{r}'|} d\vec{r}',$$

where q_A is the nuclear charge of atom A, and $\vec{R}_A$ is the coordinate of atom A. The contour maps are plotted at the order of ± 0.001, ± 0.002, ± 0.004, ± 0.008, ± 0.02, ± 0.04, ± 0.08, ± 0.2, ± 0.4 a.u. The negative polarization is shown in the red color, while the positive polarization is shown in the blue color.

3. Results and discussion

3.1. Ground-state geometry and N—H tautomers

The investigated molecules including the unsubstituted and symmetrically octakis(methoxycarbonyl/methyloxy)-substituted metal-free phthalocyanines and their Zinc complexes are shown in Scheme 1. Among the metal-free phthalocyanines, $H_2[Pc(\beta\text{-OMe})_6(\beta\text{-COOMe})_2]$, $H_2[Pc(\beta\text{-OMe})_4(\beta\text{-COOMe})_4\text{-}trans]$, and $H_2[Pc(\beta\text{-OMe})_2(\beta\text{-COOMe})_6]$ have N—H tautomers. Fig. 1 shows the different tautomeric forms of these three metal-free substituented phthalocyanines and the relative energies of their optimized structures. Throughout this text, we will use the orientation of the hydrogen atoms to unambiguously define the different tautomeric forms of these three metal-free substituented phthalocyanines. As can be found, if the energy of T_{ox} for tautomers is considered as 0.0 kcal/mol, the energy of T_{oy} is 1.7 kcal/mol for the N—H tautomer $H_2[Pc(\beta\text{-OMe})_6(\beta\text{-COOMe})_2]$, 3.5 kcal/mol for $H_2[Pc(\beta\text{-OMe})_4(\beta\text{-COOMe})_4\text{-}trans]$, and 1.8 kcal/mol for $H_2[Pc(\beta\text{-OMe})_2(\beta\text{-COOMe})_6]$, respectively, revealing the slight energy difference between the relative N—H tautomers. According to the

Boltzmann distribution $N_i = Ng_ie^{-\varepsilon_i/kT}/\sum_i g_ie^{-\varepsilon_i/kT}$, the ratio of $N(T_{ox})$: $N(T_{oy})$ is about 17.2: 1 for $H_2[Pc(\beta\text{-OMe})_6(\beta\text{-COOMe})_2]$, 364: 1 for $H_2[Pc(\beta\text{-OMe})_4(\beta\text{-COOMe})_4\text{-}trans]$, and 21.2: 1 for $H_2[Pc(\beta\text{-OMe})_2(\beta\text{-COOMe})_6]$ at the room temperature of 300 K, suggesting that T_{ox} tautomer is the dominant isomer. These small energy differences can be ascribed to the acidity of the transferred hydrogen atoms and the transferred distance difference arisen from the electron-withdrawing or -donating substituents according to pervious investigations [36–38]. As a consequence, only T_{ox} tautomers are taken into accounts in the following investigations on the basis of considering the time efficiency.

The selected geometrical features including bond lengths, bond angles, and molecular symmetries of the investigated molecules are collected in Fig. S3 (Supporting Information). In particular, Fig. S3a (Supporting Information) compares the calculated structural parameters of H_2Pc and ZnPc with those revealed by single crystal X-ray diffraction analysis [39,40]. As can be seen, the largest difference of atom distance and bond angle between the calculated and experimental data is only 0.04 Å for N_{inner}—Zn and $2.1°$ for C_γ—N_{meso}—C_8 in ZnPc, respectively, indicating the reliable simulated molecular structures at the present level. Most of the geometrical parameters of the structures are unremarkable. The same as the β-substituted phthalocyanines reported previously [7], the phthalocyanine core of our investigated molecules possess an almost planar structure based on the geometrical optimizations. In addition, the β-attached methyloxy units keep almost coplanar with the phthalocyanine core, while the two oxygen atoms of the β-attached methoxycarbonyl groups are situated on either side of the phthalocyanine core, same as the single crystal structures [41,42].

3.2. Fragment charge distribution and electrostatic potentials

Fragment charge distribution is calculated using full natural bond orbital (NBO) analysis, Tables 1 and 2. For the purpose of comparative studies, the relative NBO charges are also given in parentheses, using the fragment charges of $M[Pc(\beta\text{-COOMe})_8]$ ($M = Zn, 2H$) as benchmarks.

For the symmetrical derivatives of $Zn[Pc(\beta\text{-COOMe})_8]$ and $Zn[Pc(\beta\text{-OMe})_8]$, the electron density distributed on their β-methoxycarbonyl attached isoindole fragment and β-methyloxy attached isoindole fragment is +0.07 and +0.09 e, respectively, Table 1. In a similar manner, the β-methyloxy attached isoindole fragment electron density for $H_2[Pc(\beta\text{-OMe})_8]$ is also lower than that for $H_2[Pc(\beta\text{-COOMe})_8]$, Table 2, indicating the higher electronegativity of methoxycarbonyl group in comparison with methyloxy group.

As also shown in Table 1, the electron density movement of the unsymmetrical compounds $Zn[Pc(\beta\text{-OMe})_{2n}(\beta\text{-COOMe})_{8-2n}]$ ($n = 1, 2,$ and 3) is also influenced by the peripheral substituents. The electron density at the β-methyloxy attached isoindole fragment of $Zn[Pc(\beta\text{-OMe})_{2n}(\beta\text{-COOMe})_{8-2n}]$ ($n = 1, 2,$ and 3) locates in the range of +0.11 to +0.17e, which is lower than that for the symmetrical benchmark $Zn[Pc(\beta\text{-COOMe})_8]$. As expected, the electron density at the β-methoxycarbonyl attached isoindole fragment for $Zn[Pc(\beta\text{-OMe})_{2n}(\beta\text{-COOMe})_{8-2n}]$ ($n = 1, 2,$ and 3) in the range from -0.04 to +0.05 e is higher than that for $Zn[Pc(\beta\text{-COOMe})_8]$. These results clearly reveal the electron density movement from the β-methyloxy attached isoindole fragment to the β-methoxycarbonyl attached isoindole fragment in these unsymmetrical phthalocyanine compounds and form the mechanism of push–pull effect for $Zn[Pc(\beta\text{-OMe})_{2n}(\beta\text{-COOMe})_{8-2n}]$ ($n = 1, 2,$ and 3). This is also true for the metal-free analogues $H_2[Pc(\beta\text{-OMe})_{2n}(\beta\text{-COOMe})_{8-2n}]$ ($n = 0, 1, 2, 3,$ and 4).

Table 1
Calculated fragment charge distribution of Zn[Pc(β-OMe)$_{2n}$(β-COOMe)$_{8-2n}$] ($n = 0, 1, 2, 3,$ and 4) using full natural bond orbital (NBO) analysis.

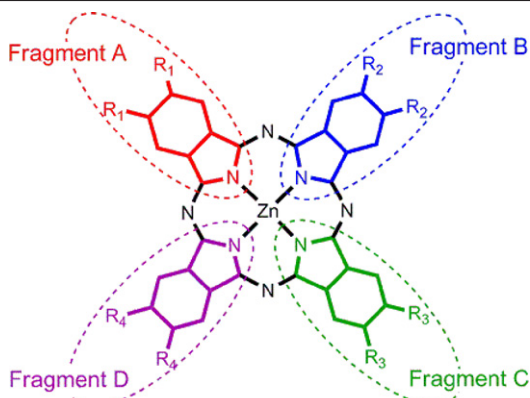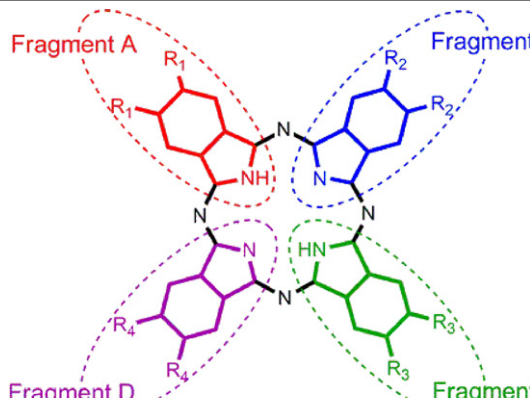|		Fragment A	Fragment B	Fragment C	Fragment D
Zn[Pc(β-OMe)$_8$]	R$_1$=R$_2$=R$_3$=R$_4$=OMe	+0.09 e (+0.02 e)	+0.09 e (+0.02 e)	+0.09 e (+0.02 e)	+0.09 e (+0.02 e)
Zn[Pc(β-OMe)$_6$(β-COOMe)$_2$]	R$_1$=R$_2$=R$_3$=OMe R$_4$=COOMe	+0.12 e (+0.05 e)	+0.14 e (+0.07 e)	+0.11 e (+0.04 e)	−0.04 e (−0.11 e)
Zn[Pc(β-OMe)$_4$(β-COOMe)$_4$-*cis*]	R$_1$=R$_2$=OMe R$_3$=R$_4$=COOMe	+0.15 e (+0.08 e)	+0.16 e (+0.09 e)	+0.03 e (−0.04 e)	−0.01 e (−0.08 e)
Zn[Pc(β-OMe)$_4$(β-COOMe)$_4$-*trans*]	R$_1$=R$_3$=OMe R$_2$=R$_4$=COOMe	+0.14 e (+0.07 e)	+0.02 e (−0.05 e)	+0.14 e (+0.07 e)	+0.02 e (−0.05 e)
Zn[Pc(β-OMe)$_2$(β-COOMe)$_6$]	R$_1$=OMe R$_2$=R$_3$=R$_4$=COOMe	+0.17 e (+0.10 e)	+0.04 e (−0.03 e)	+0.03 e (−0.04 e)	+0.05 e (−0.02 e)
Zn[Pc(β-COOMe)$_8$]	R$_1$=R$_2$=R$_3$=R$_4$=COOMe	+0.07 e (0.00 e)	+0.07 e (0.00 e)	+0.07 e (0.00 e)	+0.07 e (0.00 e)

Table 2
Calculated fragment charge distribution of H$_2$[Pc(β-OMe)$_{2n}$(β-COOMe)$_{8-2n}$] ($n = 0, 1, 2, 3, 4$) using full natural bond orbital (NBO) analysis.

		Fragment A	Fragment B	Fragment C	Fragment D
H$_2$[Pc(β-OMe)$_8$]	R$_1$=R$_2$=R$_3$=R$_4$=OMe	+0.79 e (+0.02 e)	+0.21 e (+0.01 e)	+0.79 e (+0.02 e)	+0.21 e (+0.01 e)
H$_2$[Pc(β-OMe)$_6$(β-COOMe)$_2$]	R$_1$=R$_2$=R$_3$=OMe R$_4$=COOMe	+0.83 e (+0.06 e)	+0.24 e (+0.04 e)	+0.82 e (+0.05 e)	+0.10 e (−0.10 e)
H$_2$[Pc(β-OMe)$_4$(β-COOMe)$_4$-*cis*]	R$_1$=R$_2$=OMe R$_3$=R$_4$=COOMe	+0.86 e (+0.09 e)	+0.27 e (+0.07 e)	+0.70 e (−0.07 e)	+0.14 e (−0.06 e)
H$_2$[Pc(β-OMe)$_4$(β-COOMe)$_4$-*trans*]	R$_1$=R$_3$=OMe R$_2$=R$_4$=COOMe	+0.85 e (+0.08 e)	+0.14 e (−0.06 e)	+0.85 e (+0.08 e)	+0.14 e (−0.06 e)
H$_2$[Pc(β-OMe)$_2$(β-COOMe)$_6$]	R$_1$=OMe R$_2$=R$_3$=R$_4$=COOMe	+0.88 e (+0.11 e)	+0.16 e (−0.04 e)	+0.74 e (−0.03 e)	+0.17 e (−0.03 e)
H$_2$[Pc(β-COOMe)$_8$]	R$_1$=R$_2$=R$_3$=R$_4$=COOMe	+0.77 e (0.0 e)	+0.20 e (0.0 e)	+0.77 e (0.0 e)	+0.20 e (0.0 e)

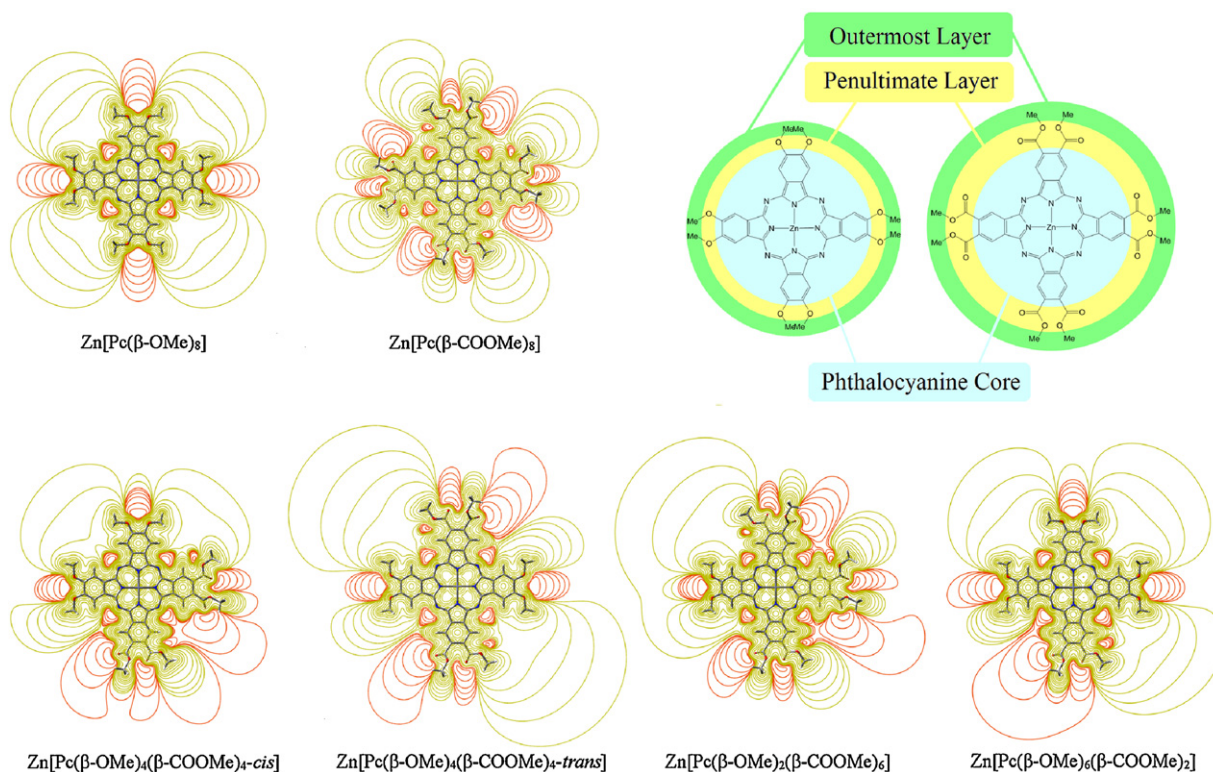**Fig. 2.** The electronic potential maps of $Zn[Pc(\beta\text{-}OMe)_{2n}(\beta\text{-}COOMe)_{8-2n}]$ ($n = 0, 1, 2, 3,$ and 4).

To visualize the electronic effects, the electrostatic potentials (EPs) of the whole series of $Zn[Pc(\beta\text{-}OMe)_{2n}(\beta\text{-}COOMe)_{8-2n}]$ ($n = 0,$ 1, 2, 3, 4) were also calculated and plotted in the plane of phthalocyanine skeleton, Fig. 2. As long as the EP maps of symmetrical $Zn[Pc(\beta\text{-}OMe)_8]/Zn[Pc(\beta\text{-}COOMe)_8]$ are concerned, the negative polarization (red) of the electron-withdrawing oxygen atoms and the positive polarization (blue) of the peripheral methyl groups are alternately arranged. Due to the more intense electronegativity of methoxycarbonyl group, the negative polarization area of $Zn[Pc(\beta\text{-}COOMe)_8]$ is obviously broader than $Zn[Pc(\beta\text{-}OMe)_8]$. It must be pointed out that the outermost "molecular surface" for both $Zn[Pc(\beta\text{-}COOMe)_8]$ and $Zn[Pc(\beta\text{-}OMe)_8]$ is occupied by the electron-donating methyl group, while the electron-withdrawing oxygen atoms and carboxyl groups are locating at the penultimate layer of the molecules, leading to most of the outer space with positive polarization nature for both $Zn[Pc(\beta\text{-}COOMe)_8]$ and $Zn[Pc(\beta\text{-}OMe)_8]$. The sole significant difference in the outer space between $Zn[Pc(\beta\text{-}COOMe)_8]$ and $Zn[Pc(\beta\text{-}OMe)_8]$ is that the negative polarization area for the former compound is a little broader than the latter one, revealing the increasing tendency to attract positively charged groups for $Zn[Pc(\beta\text{-}COOMe)_8]$.

In the case that two different kinds of electron-donating and electron-withdrawing substituents are introduced onto the phthalocyanine periphery in an unsymmetrical manner, the electrostatic potentials (EPs) of $Zn[Pc(\beta\text{-}OMe)_{2n}(\beta\text{-}COOMe)_{8-2n}]$ ($n = 1,$ 2, and 3) are also unsymmetrically distributed in the space near the molecule. As expected, the negative polarization area is close to the β-methoxycarbonyl attached isoindole fragments, while the positive polarization area close to the β-methyloxy attached isoindole fragments. The intensity of positive polarization is in consistent with the electron density of corresponding isoindole fragment. For example, Fragment C of $Zn[Pc(\beta\text{-}OMe)_6(\beta\text{-}COOMe)_2]$ has the largest electron density ($-0.04e$) among $Zn[Pc(\beta\text{-}COOMe)_{2n}(\beta\text{-}COOMe)_{8-2n}]$ ($n = 0, 1, 2, 3,$ and 4), resulting in the most intense

positive polarization around this fragment among all these compounds, Table 1.

3.3. Molecular orbitals

To gain further insights into the electronic structures, molecular orbitals (MO) were calculated using BPW91 method with the same basis sets as the geometric optimizations. It is noteworthy that the orbital distributions and energy levels for the series of metal-free phthalocyanines are similar to their zinc counterparts.

Fig. 3 shows the energy levels of frontier molecular orbitals (six highest occupied orbitals and two lowest unoccupied orbitals) and energy gaps between LUMO and HOMO. The LUMO + 1 and LUMO energies of the symmetrical phthalocyaninato zinc complexes ZnPc, $Zn[Pc(\beta\text{-}OMe)_8]$, and $Zn[Pc(\beta\text{-}COOMe)_8]$ are completely degenerated due to their high molecular symmetry. In comparison with ZnPc, the energy of LUMO/HOMO of $Zn[Pc(\beta\text{-}OMe)_8]$ increases by 0.41/0.42 eV, while that for $Zn[Pc(\beta\text{-}COOMe)_8]$ decreases by 0.71/0.66 eV, respectively, indicating more distinct effects of the electron-withdrawing methoxycarbonyl group on the frontier molecular orbital energies than the electron-donating methyloxy group.

As expected, introducing different number of methyloxy and methoxycarbonyl groups onto the phthalocyanine periphery in an unsymmetrical manner destroys the degeneracy of LUMOs of symmetrical phthalocyanine derivatives, resulting in split LUMO + 1 and LUMO for unsymmetrical phthalocyanine compounds. In terms of $\Delta E_{(LUMO+1)\text{-}(LUMO)}$ energy gap, the splitting degree of LUMO + 1 and LUMO of unsymmetrical phthalocyaninato zinc compounds increases in the order of $Zn[Pc(\beta\text{-}OMe)_4(\beta\text{-}COOMe)_4\text{-}cis]$ (0.02 eV) < $Zn[Pc(\beta\text{-}OMe)_2(\beta\text{-}COOMe)_6]$ (0.09 eV) < $Zn[Pc(\beta\text{-}OMe)_6(\beta\text{-}COOMe)_2]$ (0.11 eV) < $Zn[Pc(\beta\text{-}OMe)_4(\beta\text{-}COOMe)_4\text{-}trans]$ (0.20 eV). It is worth noting that more significant splitting occurs in the LUMOs of metal-free phthalocyanine compounds due to
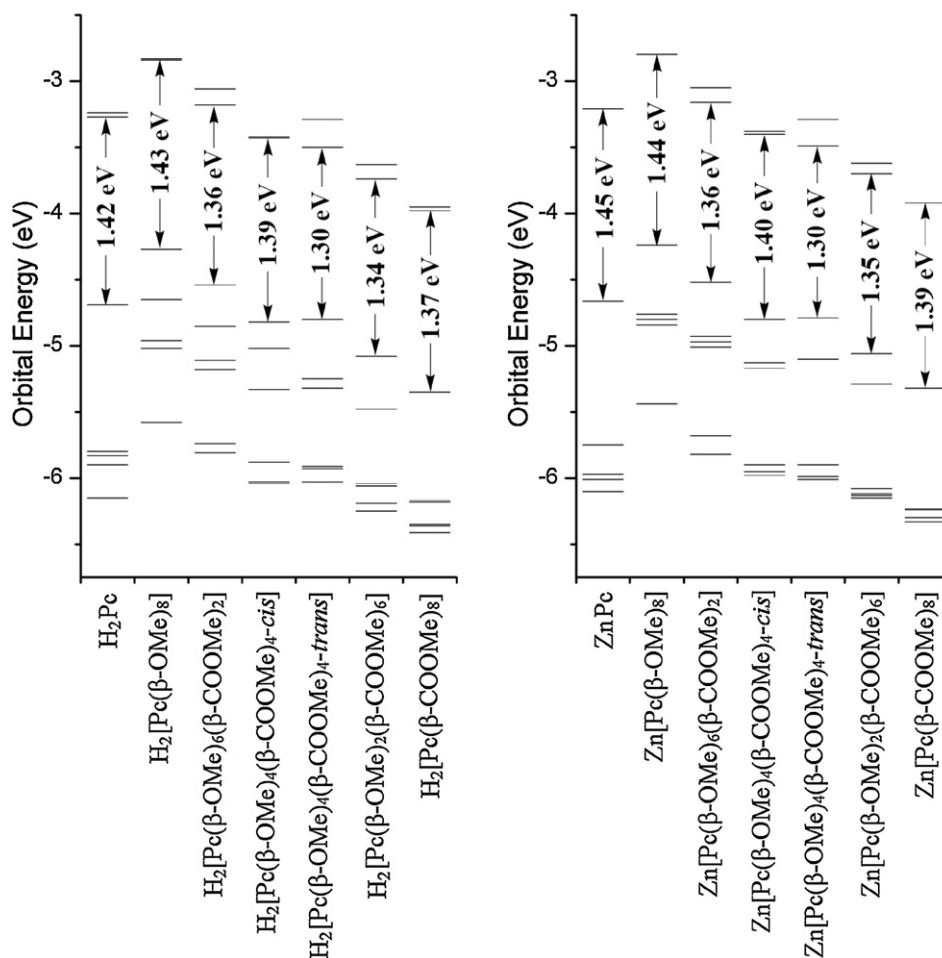
Fig. 3. The energy levels of frontier molecular orbitals (six occupied orbitals and two unoccupied orbitals) and energy gaps between LUMO and HOMO.
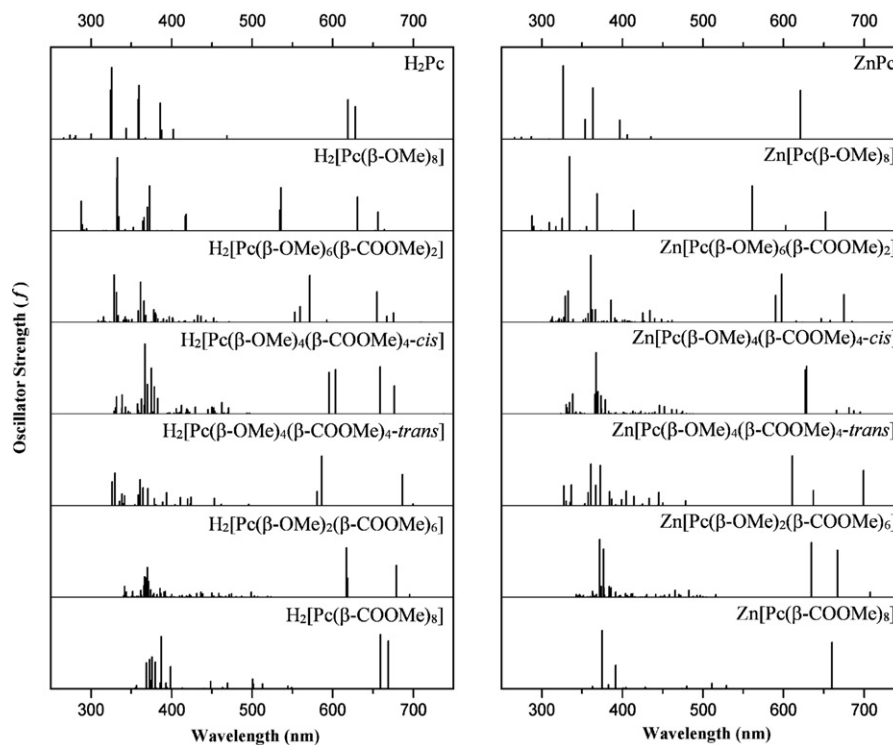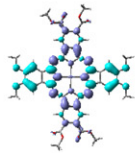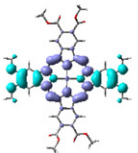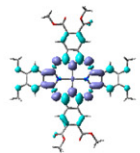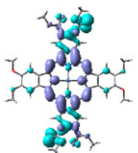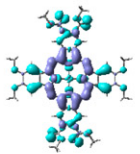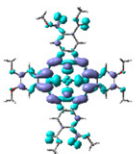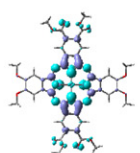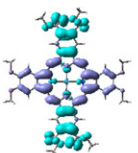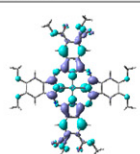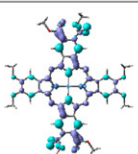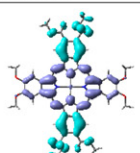

Fig. 4. Simulated electronic absorption spectra of $M[Pc(\beta-OMe)_{2n}(\beta-COOMe)_{8-2n}]$ (M = 2H, Zn; n = 0, 1, 2, 3, and 4).

Table 3
Electron density difference plots of electron transitions (isovalue: 5.0×10^{-4} e×a.u.^{3}) with Zn[Pc(β-OMe)$_4$(β-COOMe)$_4$]-*trans* as representative. Electron densities move from the green area to the blue area. Excited states with less than 30,000 cm^{-1} and configurations which contribute more than 5% are shown (Assignment: H = HOMO, L = LUMO, L + 1 = LUMO + 1, H − 1 = HOMO − 1, etc.).

Zn[Pc(β-OMe)$_4$(β-COOMe)$_4$]-*trans*

699 nm
Main Transitions:
H→L(82%)
H-1→L+1(14%)

$\Phi(^1A \to {}^1B^*) \approx 0.64\Psi_{H \to L} - 0.26\Psi_{H-1 \to L+1}$

637 nm
H-1→L+1(85%)
H→L (12%)

$\Phi(^1A \to {}^1B^*) \approx 0.65\Psi_{H-1 \to L+1} + 0.24\Psi_{H \to L}$

611 nm
H→L+1(83%)
H-1→L(9%)
H-9→L(6%)

$\Phi(^1A \to {}^1B^*) \approx 0.64\Psi_{H \to L+1} - 0.21\Psi_{H-1 \to L} - 0.17\Psi_{H-9 \to L}$

478 nm
H-5→L(96%)

$\Phi(^1A \to {}^1B^*) \approx 0.69\Psi_{H-5 \to L}$

445 nm
H-7→L(52%)
H-5→L+1(28%)
H-10→L(11%)

$\Phi(^1A \to {}^1B^*) \approx 0.51\Psi_{H-7 \to L} - 0.37\Psi_{H-5 \to L+1} - 0.23\Psi_{H-10 \to L}$

405 nm
H-10→L+1(68%)
H-7→L+1(11%)
H-9→L(7%)
H→L+4(6%)

$\Phi(^1A \to {}^1B^*) \approx 0.58\Psi_{H-10 \to L+1} + 0.24\Psi_{H-7 \to L+1} - 0.18\Psi_{H-9 \to L} + 0.17\Psi_{H \to L+4}$

372 nm
H-9→L(45%)
H-15→L+1(10%)
H-17→L+1(8%)

$\Phi(^1A \to {}^1B^*) \approx 0.48\Psi_{H-9 \to L} - 0.22\Psi_{H-15 \to L+1} + 0.20\Psi_{H-17 \to L+1}$

367 nm
H-15→L+1(84%)

$\Phi(^1A \to {}^1B^*) \approx 0.65\Psi_{H-15 \to L+1}$

361 nm
H-17→L(40%)
H-9→L+1(37%)
H-1→L+5(10%)

$\Phi(^1A \to {}^1B^*) \approx 0.45\Psi_{H-17 \to L} - 0.43\Psi_{H-9 \to L+1} + 0.22\Psi_{H-1 \to L+5}$

337 nm
H-17→L(27%)
H-4→L+2(17%)
H-9→L+1(14%)
H→L+8(9%)
H-6→L+2(9%)

$\Phi(^1A \to {}^1B^*) \approx 0.37\Psi_{H-17 \to L} + 0.29\Psi_{H-4 \to L+2} + 0.27\Psi_{H-9 \to L+1} + 0.22\Psi_{H \to L+8} - 0.21\Psi_{H-6 \to L+2}$

327 nm
H-17→L+1(59%)
H-19→L+1(16%)

$\Phi(^1A \to {}^1B^*) \approx 0.54\Psi_{H-17 \to L+1} - 0.28\Psi_{H-9 \to L+1}$

their further lowered molecular symmetry associated with the two inner hydrogen atoms. The $\Delta E_{(LUMO+1)-(LUMO)}$ values of the series of metal-free phthalocyanines, increase in the order of H$_2$[Pc(β-OMe)$_8$] (0.01 eV) < H$_2$[Pc(β-OMe)$_4$(β-COOMe)$_4$-*cis*] (0.02 eV) < H$_2$Pc (0.03 eV) = H$_2$[Pc(β-OMe)$_8$] (0.03 eV) < H$_2$[Pc(β-OMe)$_2$(β-COOMe)$_6$] (0.11 eV) < H$_2$[Pc(β-OMe)$_6$(β-COOMe)$_2$] (0.12 eV) < H$_2$[Pc(β-OMe)$_4$(β-COOMe)$_4$-*trans*] (0.21 eV).

In unsymmetrical phthalocyaninato zinc complexes, both the LUMOs and HOMO energies are always lower than the corresponding orbital energies of Zn[Pc(β-OMe)$_8$] but higher than those of Zn[Pc(β-COOMe)$_8$] due to the combined effect from both

electron-donating and withdrawing substituents. In general, the energy levels of LUMOs and HOMO decrease along with decreasing (increasing) the number of peripheral electron-donating methyloxy (electron-withdrawing methoxycarbonyl) substituents. The LUMO-HOMO gaps of the unsymmetrical phthalocyaninato zinc complexes were revealed in the range of 1.30 eV to 1.40 eV according to our calculations, which is a bit of smaller than those for the symmetrical phthalocyaninato zinc complexes ranging from 1.39 eV to 1.45 eV. Despite the same number and type of substitutes for Zn[Pc(β-OMe)$_4$(β-COOMe)$_4$-*cis*] and Zn[Pc(β-OMe)$_4$(β-COOMe)$_4$-*trans*], the large difference in the LUMO-HOMO

gap could be observed, 1.40 eV for Zn[Pc(β-OMe)$_4$(β-COOMe)$_4$-*cis*] and 1.30 eV for Zn[Pc(β-OMe)$_4$(β-COOMe)$_4$-*trans*], due to the different splitting degree of the LUMO + 1 and LUMO between these two compounds [43].

3.4. Photon-induced electron transference and microscopic mechanism of UV–vis spectra

Fig. 4 shows the simulated electronic absorption spectra of the investigated methyloxy and methoxycarbonyl substituented metal-free and zinc phthalocyanines calculated at the same level of the electronic structure. In addition, the nature of the electronic transitions for the main absorption bands is summarized in Tables S3a and S3b (Supporting Information). As can be found, regardless of the molecular symmetry, all the substituted phthalocyanines M[Pc(β-OMe)$_{2n}$(β-COOMe)$_{8-2n}$] (M = 2H, Zn; *n* = 0, 1, 2, 3, and 4) show typical Soret and Q-bands in the range of 300–450 and 550–750 nm, respectively, in their electronic absorption spectra.

As displayed in Fig. S4 (Supporting Information), the HOMO of all the phthalocyanines shows almost identical distributions. In detail, the HOMO is mainly distributed on all the carbon atoms, while almost no distribution on the eight nitrogen atoms. According to the previous results [44,45], the absorption band originated from the electron transitions of HOMO → LUMO/LUMO + 1 is attributed to the phthalocyanine Q-band.

As for symmetrical phthalocyaninato zinc compounds, one combined Q-band is revealed at 621, 652, and 660 nm for ZnPc, Zn[Pc(β-OMe)$_8$], and Zn[Pc(β-COOMe)$_8$] due to the electron transitions of HOMO → LUMO/LUMO + 1. In contrast, their corresponding metal-free phthalocyanine analogues show two split Q-bands at 628 and 619 nm for H$_2$Pc, 657 and 631 nm for H$_2$[Pc(β-OMe)$_8$], and 669 and 659 nm for H$_2$[Pc(β-COOMe)$_8$]. As detailed above, the slight split Q-bands is generated from the non-degenerated LUMO and LUMO + 1 caused by the two inner hydrogen atoms [46].

As previously described, introducing different number of methyloxy and methoxycarbonyl groups onto the phthalocyanine periphery in an unsymmetrical manner results in obvious splitting of LUMO and LUMO + 1 for the unsymmetrically substituted phthalocyanines. As a consequence, relatively large split Q-bands have been revealed for the unsymmetrically substituted phthalocyanine compounds. The Q-band absorptions are found at 675 and 598 nm for Zn[Pc(β-OMe)$_6$(β-COOMe)$_2$], 629 and 627 nm for Zn[Pc(β-OMe)$_4$(β-COOMe)$_4$-*cis*], 699 and 611 nm for Zn[Pc(β-OMe)$_4$(β-COOMe)$_4$-*trans*], and 667 and 634 nm for Zn[Pc(β-OMe)$_2$(β-COOMe)$_6$]. In terms of the ($Q_x - Q_y$) energy, the splitting degree for the Q-bands of unsymmetrical phthalocyaninato zinc compounds increases in the order of Zn[Pc(β-OMe)$_4$(β-COOMe)$_4$-*cis*] (0.01 eV) < Zn[Pc(β-OMe)$_2$(β-COOMe)$_6$] (0.10 eV) < Zn[Pc(β-OMe)$_6$(β-COOMe)$_2$] (0.23 eV) < Zn[Pc(β-OMe)$_4$(β-COOMe)$_4$-*trans*] (0.26 eV), the same as for the splitting degree of their LUMOs. The maps of electron difference between the ground state and excited states for Q bands with Zn[Pc(β-OMe)$_4$(β-COOMe)$_4$-*trans*] as typical representative are shown in Table 3, while those for all the remaining phthalocyaninato zinc compounds are available in Table S4 (Supporting Information). For Q transitions, the electron density moves mainly from the peripheral fused-benzene ring to the tatraazaporphyrin core with obvious photon-induced electron transference from methyloxy to methoxycarbonyl groups.

The transitions for Soret bands are constructed by many π → π* electron transitions with different nature, rendering it hard to give clear assignment for these bands. As shown in Table S4, the photon-induced electron transference for Soret bands also mainly locates at the phthalocyanine core with a little contribution from the peripheral substituents.

4. Conclusions

The molecular and electronic structures together with the electronic absorption spectra of a series of peripherally methyloxy/methoxycarbonyl substituented phthalocyanines have been studied using the density functional theory (DFT) and time-dependent density functional theory (TD-DFT) methods. The effects of the electron-withdrawing and donation groups on the charge distribution and electrostatic potential have been analyzed. The significant splitting in the Q-bands for unsymmetrically substituted phthalocyanines is attributed to the non-degenerated LUMO and LUMO + 1 associated with the unsymmetrically attached peripheral methyloxy and methoxycarbonyl groups. The microscopic mechanism of the UV–vis spectra has been clarified on the basis of multi-band photon-induced electron transference.

Appendix A. Supplementary data

Supplementary data associated with this article can be found, in the online version, at doi:10.1016/j.jmgm.2011.11.005.

References

[1] J. Jiang, Functional phthalocyanine molecular materials, in: D.M.P. Mingos (Ed.), Struct. Bond., vol. 135, Springer Press, Heidelberg, 2010, pp. 1–321.
[2] M.-S. Liao, T. Kar, S.M. Gorun, S. Scheiner, Effects of peripheral substituents and axial ligands on the electronic structure and properties of iron phthalocyanine, Inorg. Chem. 43 (2004) 7151–7161.
[3] N. Kobayashi, H. Ogata, N. Nonaka, E.A. Luk'yanets, Effect of peripheral substitution on the electronic absorption and fluorescence spectra of metal-free and zinc phthalocyanines, Chem. Eur. J. 9 (2003) 5123–5134.
[4] G. de la Torre, P. Vázquez, F. Agulló-López, T. Torres, Role of structural factors in the nonlinear optical properties of phthalocyanines and related compound, Chem. Rev. 104 (2004) 3723–3750.
[5] E. Ben-Hur, W.S. Chan, Phthalocyanines in photobiology and their medical applications, in: K.M. Kadish, K.M. Smith, P. Guilard (Eds.), The Porphyrin Handbook, vol. 19, Academic Press, San Diego, 2003, pp. 1–35.
[6] X. Li, H. Wang, H. Wu, Phthalocyanines and their analogs applied in dye-sensitized solar cell, in: D.M.P. Mingos (Ed.), Struct. Bond., vol. 135, Springer Press, Heidelberg, 2010, pp. 229–322.
[7] L. Wan, D. Qi, Y. Zhang, J. Jiang, Controlling the directionality of the charge transfer in phthalocyaninato zinc sensitized solar cell: density functional theory studies, Phys. Chem. Chem. Phys. 13 (2011) 1639–1648.
[8] R. Ma, P. Guo, H. Cui, X. Zhang, M.K. Nazeeruddin, M. Grätzel, Substituent effect on the meso-substituted porphyrins: theoretical screening of sensitizer candidates for dye-sensitized solar cells, J. Phys. Chem. A 113 (2009) 10119–10124.
[9] P.Y. Reddy, L. Giribabu, C. Lyness, H.J. Snaith, C. Vijaykumar, M. Chandrasekharam, M. Lakshmikantam, J.-H. Yum, K. Kalyanasundaram, M. Grätzel, M.K. Nazeeruddin, Efficient sensitization of nanocrystalline TiO$_2$ films by a near-IR-absorbing unsymmetrical zinc phthalocyanine, Angew. Chem. Int. Ed. 46 (2007) 373–376.
[10] K.S. Suslick, C.-T. Chen, G.R. Meredith, L.-T. Cheng, Push–pull porphyrins as nonlinear optical materials, J. Am. Chem. Soc. 114 (1992) 6928–6930.
[11] Z. Bai, Y. Gao, P. Zhu, Y. Bian, J. Jiang, Novel pathway to synthesize unsymmetrical 2,3,9,10,16,17,23-heptakis(alkoxyl)-24-mono(dimethylaminoalkoxyl)phthalocyanines, Inorg. Chem. 49 (2010) 9005–9011.
[12] E.M. Maya, C. García, E.M. García-Frutos, P. Vázquez, T. Torres, Synthesis of novel push–pull unsymmetrically Substituted alkynyl phthalocyanines, J. Org. Chem. 65 (2000) 2733–2739.
[13] A. Sastre, B. Rey, T. Torres, Synthesis of novel unsymmetrically substituted push–pull phthalocyanines, J. Org. Chem. 61 (1996) 8591–8597.

[14] J. Mack, N. Kobayashi, Low symmetry phthalocyanines and their analogues, Chem. Rev. 111 (2011) 281–321.

[15] H. Miwa, K. Ishii, N. Kobayashi, Electronic structures of zinc and palladium tetraazaporphyrin derivatives controlled by fused benzo rings, Chem. Eur. J. 10 (2004) 4422–4435.

[16] K. Ishii, H. Itoya, H. Miwa, M. Fujitsuka, O. Ito, N. Kobayashi, Relationship between symmetry of porphyrinic π-conjugated systems and singlet oxygen ($^1\Delta_g$) yields: low-symmetry tetraazaporphyrin derivatives, J. Phys. Chem. A 109 (2005) 5781–5787.

[17] P. Ma, Z. Bai, Y. Gao, Q. Wang, J. Kan, Y. Bian, J. Jiang, Helical nano-structures self-assembled from dimethylaminoethyloxy-containing unsymmetrical octakis-substituted phthalocyanine derivatives, Soft Matter 7 (2011) 3417–3422.

[18] N. Tian, P. Ma, Q. Wang, X. Zhang, J. Jiang, M. Bai, Ring-shaped *J*-type and star-shaped *H*-type nanostructures of an unsymmetrical (phthalocyaninato)zinc complex, Eur. J. Inorg. Chem. (2011) 1466–1472.

[19] P. Ma, J. Kan, Y. Zhang, C. Huang, Y. Bian, Y. Chen, N. Kobayashi, J. Jiang, The first solution-processable n-type phthalocyaninato copper semiconductor: tuning the semiconducting nature via peripheral electron-withdrawing octyloxycarbonyl substituents, J. Mater. Chem. 21 (2011) 18552–18559.

[20] S. Yan, Y. Bu, Z. Cao, P. Li, Coupling character between imidazole and imidazole cation: implication for the coupling modes of biomolecular residues, J. Phys. Chem. A 108 (2004) 7038–7049.

[21] D. Qi, Y. Zhang, L. Zhang, J. Jiang, Structures and spectroscopic properties of fluoroboron-subtriazaporphyrin derivatives: density functional theory approach on the benzo-fusing effect, J. Phys. Chem. A 114 (2010) 1931–1938.

[22] L. Wan, Y. Zhang, D. Qi, J. Jiang, Structures and properties of 1,8,15,22-tetrasubstituted phthalocyaninato zinc and nickel complexes: substitution and axially coordination effects study based on density functional theory calculations, J. Mol. Graphics Modell. 28 (2010) 842–851.

[23] V.N. Nemykin, R.G. Hadt, R.V. Belosludov, H. Mizuseki, Y. Kawazoe, Influence of molecular geometry, exchange-correlation functional, and solvent effects in the modeling of vertical excitation energies in phthalocyanines using time-dependent density functional theory (TDDFT) and polarized continuum model TDDFT methods: can modern computational chemistry methods explain exper-imental controversies? J. Phys. Chem. A 111 (2007) 12901–12913.

[24] S.U. Lee, J.C. Kim, H. Mizuseki, Y. Kawazoe, The origin of the halogen effect on the phthalocyanine green pigments, Chem. Asian J. 5 (2010) 1341–1346.

[25] D. Qi, L. Zhang, Y. Zhang, Y. Bian, J. Jiang, Nature of the intense near-IR absorp-tion and unusual broad UV–visible–NIR spectra of azulenocyanines: density functional theory studies, J. Phys. Chem. A 114 (2010) 13411–13417.

[26] A.D. Becke, Density-functional thermochemistry. III. The role of exact exchange, J. Chem. Phys. 98 (1993) 5648–5652.

[27] C. Lee, W. Yang, R.G. Parr, Development of the colle-salvetti correlation-energy formula into a functional of the electron density, Phys. Rev. B 37 (1988) 785–789.

[28] C. Peng, P.Y. Ayala, H.B. Schlegel, M.J. Frisch, Using redundant internal coor-dinates to optimize equilibrium geometries and transition states, J. Comput. Chem. 17 (1996) 49–56.

[29] A.E. Reed, L.A. Curtiss, F. Weinhold, Intermolecular interactions from a natural bond orbital, donor–acceptor viewpoint, Chem. Rev. 88 (1988) 899–926.

[30] J.E. Carpenter, F. Weinhold, Analysis of the geometry of the hydroxymethyl rad-ical by the different hybrids for different spins natural bond orbital procedure, J. Mol. Struct. (THEOCHEM) 169 (1988) 41–62.

[31] M.J. Frisch, G.W. Trucks, H.B. Schlegel, G.E. Scuseria, M.A. Robb, J.R. Cheese-man, J.A. Montgomery Jr., T. Vreven, K.N. Kudin, J.C. Burant, J.M. Millam, S.S. Iyengar, J. Tomasi, V. Barone, B. Mennucci, M. Cossi, G. Scalmani, N. Rega, G.A. Petersson, H. Nakatsuji, M. Hada, M. Ehara, K. Toyota, R. Fukuda, J. Hasegawa, M. Ishida, T. Nakajima, Y. Honda, O. Kitao, H. Nakai, M. Klene, X. Li, J.E. Knox, H.P. Hratchian, J.B. Cross, V. Bakken, C. Adamo, J. Jaramillo, R. Gomperts, R.E. Strat-mann, O. Yazyev, A.J. Austin, R. Cammi, C. Pomelli, J.W. Ochterski, P.Y. Ayala, K. Morokuma, G.A. Voth, P. Salvador, J.J. Dannenberg, V.G. Zakrzewski, S. Dapprich, A.D. Daniels, M.C. Strain, O. Farkas, D.K. Malick, A.D. Rabuck, K. Raghavachari, J.B. Foresman, J.V. Ortiz, Q. Cui, A.G. Baboul, S. Clifford, J. Cioslowski, B.B. Ste-fanov, G. Liu, A. Liashenko, P. Piskorz, I. Komaromi, R.L. Martin, D.J. Fox, T. Keith, M.A. Al-Laham, C.Y. Peng, A. Nanayakkara, M. Challacombe, P.M.W. Gill, B. John-son, W. Chen, M.W. Wong, C. Gonzalez, J.A. Pople, Gaussian03, Revision B. 05, Gaussian, Inc., Pittsburgh, PA, 2003.

[32] A.D. Becke, Density-functional exchange-energy approximation with correct asymptotic behavior, Phys. Rev. A 38 (1988) 3098–3100.

[33] J.P. Perdew, Y. Wang, Accurate and simple analytic representation of the electron-gas correlation energy, Phys. Rev. B 45 (1992) 13244–13249.

[34] S.I. Gorelsky, SWizard program, University of Ottawa, Ottawa, Canada, 2010, http://www.sg-chem.net/.

[35] S.I. Gorelsky, A.B.P. Lever, Electronic structure and spectra of ruthenium diimine complexes by density functional theory and INDO/S. Comparison of the two methods, J. Organomet. Chem. 635 (2001) 187–196.

[36] D. Qi, Y. Zhang, X. Cai, J. Jiang, M. Bai, Inner hydrogen atom transfer in benzo-fused low symmetrical metal-free tetraazaporphyrin and phthalocya-nine analogues: density functional theory studies, J. Mol. Graphics Modell. 27 (2009) 693–700.

[37] Y. Zhang, P. Yao, X. Cai, H. Xu, X. Zhang, J. Jiang, Density functional theory study of the inner hydrogen atom transfer in metal-free porphyrins: meso-sub-stitutional effects, J. Mol. Graphics Modell. 26 (2007) 319–326.

[38] X. Lu, Y. He, J. Chen, J. Wang, H. Shi, Theoretical study of the inner hydro-gen migration in the β-substituted 5,10,15,20-tetraphenylporphyrins, J. Phys. Chem. A 114 (2010) 12731–12738.

[39] J.A. Thompson, K. Murata, D.C. Miller, J.L. Stanton, W.E. Broderick, B.M. Hoff-man, J.A. Lbers, Synthesis of high-purity phthalocyanines (pc): high intrinsic conductivities in the molecular conductors $H_2(pc)I$ and $Ni(pc)I$, Inorg. Chem. 32 (1993) 3546–3553.

[40] K. Morishige, K. Araki, Crystal structures of nickel, copper and zinc naphthalo-cyanines, J. Chem. Soc., Dalton Trans. (1996) 4303–4305.

[41] R. Deshpande, L. Jiang, G. Schmidt, J. Rakovan, X. Wang, K. Wheeler, H. Wang, A concise approach to the synthesis of opp-dibenzoporphyrins through the Heck reaction, Org. Lett. 11 (2009) 4251–4253.

[42] K.M. Kadish, O.S. Finikova, E. Espinosa, C.P. Gros, G. De Stefano, A.V. Cheprakov, I.P. Beletskaya, R. Guilard, First highly distorted π-extended Fe(II) porphyrin – a unique model to elucidate factors affecting the electrochemical potentials, J. Porphyrins Phthalocyanines 8 (2004) 1062–1066.

[43] L. Zhang, D. Qi, Y. Zhang, Y. Bian, J. Jiang, Density functional theory studies on the structures and electronic communication of meso-ferrocenylporphyrins: long range orbital coupling via porphyrin core, J. Mol. Graphics Modell. 29 (2011) 717–725.

[44] J. Mack, M.J. Stillman, The Porphyrin Handbook, Vol. 16, 2003, Chapter 103, pp 43–116.

[45] C. Liu, W. Guan, P. Song, L.-K. Yan, Z. Su, Redox-switchable second-order nonlin-ear optical responses of push–pull monotetrathiafulvene-metalloporphyrins, Inorg. Chem. 48 (2009) 6548–6554.

[46] A. Zhong, Y. Zhang, Y. Bian, Structures and spectroscopic properties of nonperipherally and peripherally substituted metal-free phthalocyanines: a substitution effect study based on density functional theory calculations, J. Mol. Graphics Modell. 29 (2010) 470–480.